An age scale for new climate records from Sherman Island, West Antarctica

Isobel Rowell[1], Helena Pryer[1], Carlos Martin[2], Dieter Tetzner[2], Emily Doyle[1], Robert Mulvaney[2], and Eric Wolff[1]

[1]Department of Earth Sciences, University of Cambridge, Downing Street, Cambridge, CB2 3EQ
[2]British Antarctic Survey, High Cross, Madingley Road, Cambridge, CB3 0ET

Correspondence: Isobel Rowell (ifr21@cam.ac.uk)

Abstract. Few ice cores from the Amundsen and Bellingshausen Sea sectors of the West Antarctic Ice Sheet (WAIS) extend back in time further than a few hundred years. The WAIS is believed to be susceptible to collapse as a result of anthropogenic climate change and may have at least partially collapsed in the past. Understanding the stability of the WAIS during warm periods such as the LIG and Holocene is important. As part of the WACSWAIN project, the British Antarctic Survey's (BAS)

5   Rapid Access Isotope Drill (RAID) was deployed in 2020 on Sherman Island in the Abbott Ice Shelf. We drilled a 323 m deep borehole, with discrete samples of ice chippings collected covering the entire depth range of the drilled ice. The samples were analysed for stable water isotope composition and major ion content at BAS from 2020-2022. Using annual layer counting of chemical records, volcanic horizon identification and modelling, an age scale for the record of 1724 discrete samples is presented. The Sherman Island ice record extends back to greater than 1150 years before present, providing the oldest, continuous,

10   ice-derived palaeoclimate records for the coastal Amundsen-Bellingshausen Sea sectors to date. We demonstrate the potential for recovery of a complete Holocene climate record from Sherman Island in the future, and confidence in the ability of RAID samples to contain sufficiently resolved records for meaningful climatic interpretation.

1 Introduction

The West Antarctic Ice Sheet (WAIS) is believed to be vulnerable to collapse due to anthropogenic warming, with the potential

15   to contribute several metres to global sea level (Mercer, 1978; Oppenheimer, 1998; Edwards et al., 2019; Bamber et al., 2019; Lowry et al., 2021). Much of the WAIS is grounded in marine basins lying up to 2000 m below sea level, making it highly susceptible to mass loss as a result of marine ice sheet instability (MISI) induced by ocean warming (Joughin and Alley, 2011; Shepherd et al., 2004). The recent thinning of WAIS and Southern Antarctic Peninsula ice shelves has resulted in accelerated flow of their respective glaciers into the Bellingshausen and Amundsen Sea embayment and their grounding

20   lines have subsequently retreated over the last few decades (Konrad et al., 2018; Paolo et al., 2015; Wouters et al., 2015). Current loss of ice volume from the WAIS is dominated by loss from the Pine Island and Thwaites Glaciers (PIG and TG respectively) (Pattyn and Morlighem, 2020). Significant retreat of WAIS glaciers is underway and is identified as one of the major "tipping points" in the climate system, which could bring about irreversible WAIS collapse (Lenton et al., 2008). WAIS

Table 1. Information about the Sherman Island RAID site and drilling campaign.

Latitude (°)	Longitude (°)	Elevation (m)	Ice thickness (m)	Depth drilled (m)	No. samples
-72.67	-99.71	440	428	323.23	1724

loss has implications for other parts of the climate system, such as Antarctic sea ice coverage, albedo and freshening of the
25   Southern Ocean, highlighting the importance of research in this area (Bronselaer et al., 2018; Wunderling et al., 2020).

The WAIS is believed to have at least partially collapsed during past warm periods, including the Last Interglacial (LIG)
(DeConto and Pollard, 2016). Investigating the behaviour of the WAIS during these times provides insights into ice sheet
stability which can be used to understand and predict current and future change. The WACSWAIN project (WArm Climate
Stability of the West Antarctic ice sheet in the last INterglacial) aims to use ice core records to investigate the WAIS during
30   the LIG. An ice core on Skytrain Ice Rise (Figure 1) was successfully drilled to the bed at 651 m, results from which are
now being published (Mulvaney et al., 2021; Hoffmann et al., 2022). Drilling was carried out at a second site, on Sherman
Island, located in the Abbott Ice Shelf in between continental Antarctica and Thurston Island, close to TG and PIG (Figure
1 and Table 1). Sherman Island was chosen to provide a constraint on the Amundsen and Bellingshausen Sea sectors of the
WAIS. Drilling using the British Antarctic Survey's (BAS) Rapid Access Isotope Drill (RAID) was completed in early 2020
35   (Mulvaney et al., 2021). The RAID was chosen due to the high risk of Sherman Island not containing ice from the LIG. It
has been demonstrated the drilling and sampling techniques necessary for RAID ice do not result in significant mixing or
attenuation of stable water isotopic or chemical signals in the ice, and an identified chemical contamination problem does not
impact climatic interpretation, particularly on longer time-scales (Rowell et al., 2022). Drilling reached a depth of 323 m, out
of a total ice sheet depth of approximately 428 m, at which point the drill became stuck in the ice and the drilling campaign
40   ended (Mulvaney et al., 2021). Not reaching the bedrock is expected to significantly reduce the total possible length of the
climate records obtained, due to the exponential increase of age with depth.

There is great value in assessing the natural climate variability of the last few centuries, in order to set current and future
warming and ice sheet behaviour into recent context. Crucial to this task is assigning a reliable age scale to the ice, and this
paper addresses that for the new RAID core from Sherman Island.

45   ## 2   Drilling and measurements

A detailed description of the Sherman Island Rapid Access Isotope Drill (RAID) field campaign can be found in Mulvaney
et al. (2021). The BAS RAID (Rix et al., 2019) drilled to a depth of 323 m in five drilling days, collecting discrete samples of
ice chippings as described in Rowell et al. (2022) and Mulvaney et al. (2021).

A detailed description of the RAID lab measurements can be found in Rowell et al. (2022). In summary, stable water isotope
50   and chemistry data were collected from 1724 samples of ice chips at a resolution of 6 to 29 cm (average 19 cm). Some chemical
data had to be discarded because of contamination from the drill, but as described in Rowell et al. (2022), the remaining dataset

Figure 1. Map of West Antarctica indicating the location of the WACSWAIN drilling sites. Map generated using QGIS with the Quantarctica mapping environment (Matsuoka et al., 2021). Black lines show elevation at 1000 m interval contour lines from CryoSat-2. The markers show Sherman Island (the focus of this paper) and Skytrain Ice Rise (for reference).

appears robust and suitable for looking at annual layers and at trends in the concentration of chemical ions and the stable water isotope composition.

3 SI:RAID age scale development

55   The Sherman Island RAID age scale was produced using three methods. Annual layer counting of stable water isotopic and chemical species was carried out on the basis that the stable water isotopic composition and concentration of certain ions vary seasonally, enabling the visualisation and counting of peaks and troughs corresponding to one annual cycle, or layer, in the ice (e.g., Sigg and Neftel (1988); Sigl et al. (2016); Winstrup et al. (2019)). The layers can simply be counted from one year to the next, giving fixed depths for the summer and/or winter of the shallower, more recent years in the ice sheet. Identification

60   of large, well-dated volcanic events in the sulfate (SO_4^{2-}) record, supplemented with sulfur (S) isotope analysis to differentiate between background and volcanic samples, was conducted to date ice beyond the depth where annual layer counting was possible. Two ice thinning models were used to give an initial estimate of the age scale, assess confidence in the first two dating methods and provide an age estimation for the deepest ice. The three steps are described in further detail below.

3.0.1 Annual layer counting

Annual layer counting (Figures 2 and 3) was performed on stable water isotope ratio and chemical data plotted on a depth scale. The MATLAB programme "Matchmaker" was used for plotting multiple records together from the SI:RAID data and a nearby 20 m long SI ice core (SI:Core) and identifying corresponding peaks and troughs, placing markers and adjusting the age scale accordingly (Rasmussen et al., 2013; Tetzner et al., 2022, 2021). The species used consistently throughout annual layer counting were: deuterium ($\delta\,^2$H), methanesulfonic acid (MSA$^-$), sulfate (SO$_4^{2-}$) and sodium (Na$^+$). These species have highest values during the austral summer (December to February) because $\delta\,^2$H responds primarily to temperature and SO$_4^{2-}$ and MSA$^-$ are related to marine bio-productivity, both of which peak in the summer (Turner et al., 1995). The relative contribution of Na$^+$ seasonally to the ice appears to be inconsistent at Sherman Island, with some years seeing summer peaks corresponding to clear summer signals in the $\delta\,^2$H record and other years showing winter peaks. This variability could be representative of a site such as Sherman Island, which is close to open water sea salt contributions in the summer and then closely surrounded by salt-producing sea ice in the winter, with potential contributions from nearby Pine Island and Amundsen Sea polynyas. The contribution of Na$^+$ to the ice core site could therefore be dependent on wind direction and circulation patterns rather than seasonality. Counting was therefore supplemented with the SO$_4^{2-}$/Na$^+$ ratio in places where the seasonality of Na$^+$ was unclear.

Annual age markers from the SI:Core were used to add summer-to-summer reference points in the top 20 m of the RAID data to aid the layer counting. The SI:RAID data show similar absolute concentrations to the SI:Core, as well as closely matching annual variability throughout much of the 20 m, but with less well-defined peaks because of the lower depth resolution (Figure 2). Using the spacing of the annual layers in the top 20 m, with the SI:Core as a guide, counting was continued to 70 m using the same technique as for the top 20 m but without the assistance of the SI:Core data. It is possible that annual layer counting could have been continued below 70 m. However, the regular variations, which arguably are still seasonal variations, are difficult to distinguish from variability caused by other factors. In particular, seasonal variability in $\delta\,^2$H becomes limited below this depth. The regular peaks and troughs that are indicative of seasonal variations are formed from typically less than four data points below 70 m meaning that annual layer counting below this point cannot be considered robust.

3.0.2 Modelling ice thinning and *a priori* estimate of depth/age

Using the age scale for the top 70 m from annual layer counting, it was possible to estimate the age of deeper samples. This estimate was done in combination with an ice thinning model. Details about the model can be found in Martín et al. (2015), but we summarize here the main equations for convenience. The model neglects horizontal advection and calculates age A at a given depth d and time t as a function of the vertical velocity w as,

$$\frac{\partial A}{\partial t}(d,t) - w(d,t)\frac{\partial A}{\partial d}(d,t) = 1 \qquad 0 \le d \le H, \quad -t_0 \le t \le 0$$
$$A(d,t0) = A_0,$$
$$A(0,t) = 0, \tag{1}$$
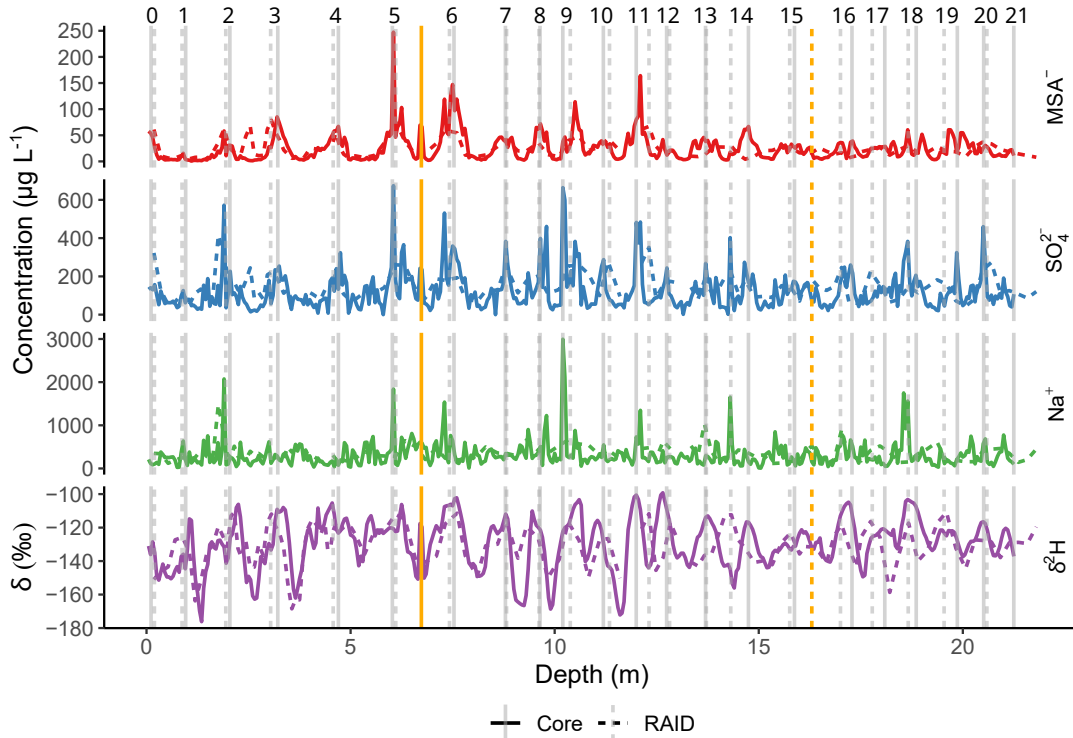
Figure 2. Annual layer counting of the top 20 m of the Sherman Island data. Counts are performed using both SI:RAID and SI:Core data. Grey age markers are placed on the assigned summer peak, with dashed lines corresponding to RAID data and solid lines corresponding to Core data. δ^2H data in ‰, all other data in $\mu g L^{-1}$. Yellow lines represent "uncertain" years in both core and RAID and are not included in either age scale.

where H is the ice thickness, and A_0 is the initial depth/age, a time t_0 before the present $t = 0$.

We further assume that in the vertical velocity we can separate the time- and depth-dependency, that there is no basal melt
95   or variation of ice thickness with time. The vertical velocity can be then written as,

$$w(d,t) = -a(t)\frac{\rho_i}{\rho(d)}\eta(d), \tag{2}$$

where ρ is the density, that is assumed uniform in time, ρ_i is the density of ice, a is the time-dependent accumulation, and
$\eta(d)$ is a function of depth, often referred as shape function, that varies between 0 at the bed and 1 at the surface. For the shape
function we use two extreme approximations. For one extreme, we use Lliboutry (1979),

100    $$\eta(d) = 1 - \frac{p+2}{p+1}\left(\frac{d}{H}\right) + \frac{1}{p+1}\left(\frac{d}{H}\right)^{p+2}, \tag{3}$$
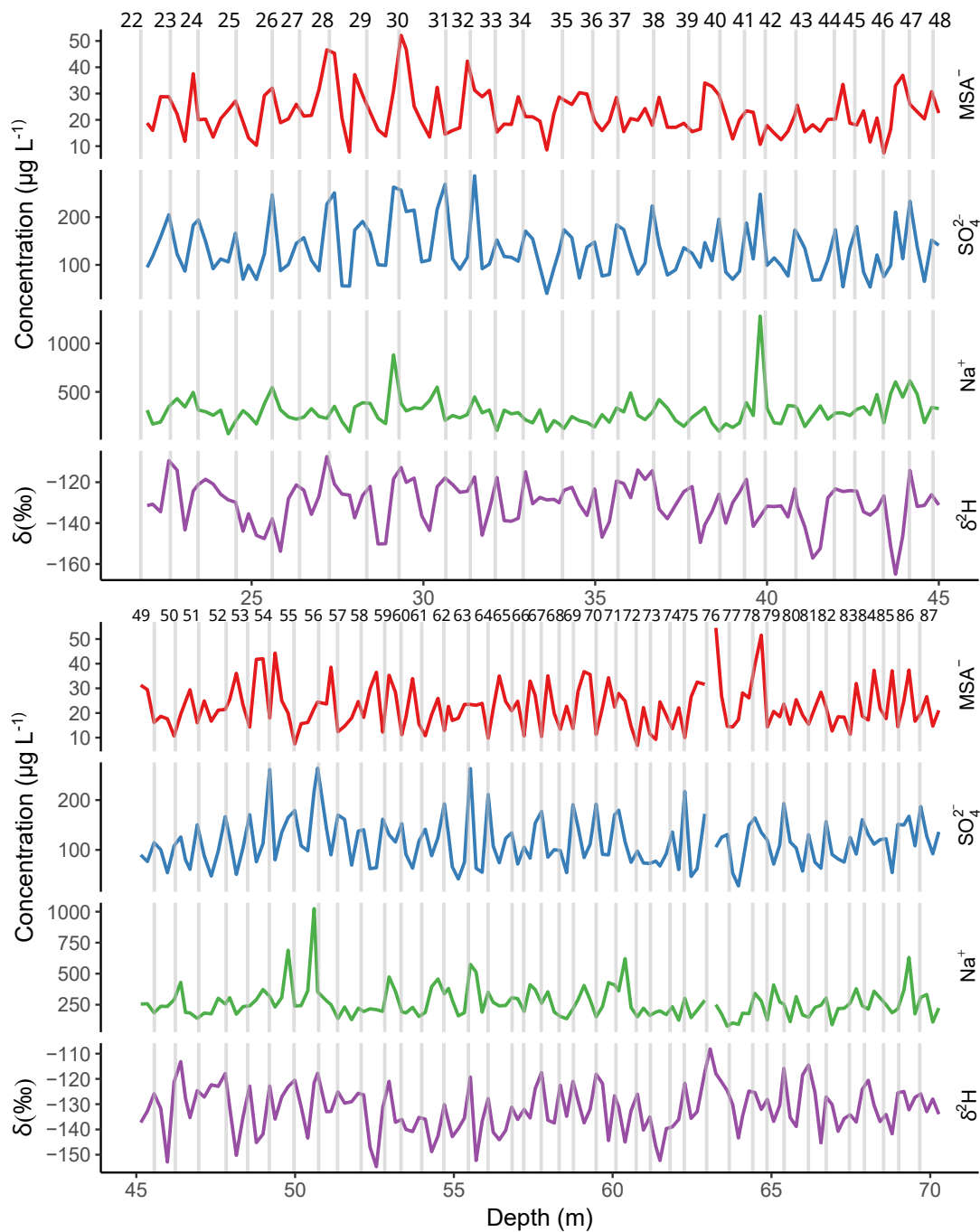
Figure 3. Annual layer counting from 20 to 70 m of the Sherman Island data. Counting is continued from 20 m with just the RAID data. Grey age markers are placed on the assigned summer peak. δ^2H data in ‰, all other data in µg L^{-1}. Y-axis ranges of panels adjusted for appropriate range of concentrations in the depth range of data shown in the panel.

where p is a parameter. The Lliboutry approximation reproduces well flow dominated by shear (Martín and Gudmundsson, 2012) and we use it to simulate ice thinning at the flanks of the ice flow divide. That is, more than a few thicknesses away from the ice flow divide that is often located near the ridge perpendicular to ice flow. On the other extreme, to represent ice flow divide conditions, we use the numerical output at the divide from the full field model of Martín and Gudmundsson (2012).

105   For our *a priori* depth/age model we assume that the accumulation is proportional to that of EPICA Dome C (Bazin et al., 2012) using the present values of accumulation at Sherman from annual layer counting. Our hypothesis is that the flow conditions can be bounded between divide flow and flank flow with $p = 3$. The results for the depth/age estimation from both extremes are in Figure 5.

3.0.3   Volcanic horizon identification

110   It became clear during our analysis that the depth/age model for flank-flow conditions is consistently better fitting our depth/date markers. We use the flank-flow depth/age model as a *prior* to guide us in the dating of the deeper samples.

The records of chemical species were closely inspected for signatures of volcanic events as explained below. Based on the *a priori* depth/age model and annual layer thickness in the top 70 m, it was clear that with a 19 cm average sample resolution, samples would continue to be annual, or greater, resolution until at least 250 m depth. Assuming the imprint of volcanic events

115   is recorded in the SO_4^{2-} concentration at Sherman Island, this sample age resolution is adequate to resolve individual volcanic events.

Large volcanic eruptions emit sulfurous gases such as sulfur dioxide (SO_2) and hydrogen sulfide (H_2S) into the atmosphere, which are oxidised and precipitated onto the ice sheets in the form of SO_4^{2-}, leaving a peak in the SO_4^{2-} concentration of the ice layer (Delmas et al., 1985). Matching volcanic peaks in the SO_4^{2-} record of ice cores with known volcanic events provides

120   an age constraint at certain depth intervals (e.g., Udisti et al. (2004); Parrenin et al. (2012); Severi et al. (2012)). The Sherman Island drill site is only 440 m above sea level and located very close to open ocean. The SO_4^{2-} record is therefore dominated by marine biogenic and sea salt sources, making volcanic peaks more difficult to identify. The total SO_4^{2-} concentration was split into sea-salt (ss) and non-sea-salt (nss) components to aid the identification of volcanic peaks, according to Equations 4 to 8.

$$[\text{nssCa}^{2+}] = [\text{Ca}^{2+}] - [ss\text{Na}^+] \cdot \text{R}_\text{m} \tag{4}$$

125   $$[ss\text{Na}^+] = [\text{Na}^+] - [nss\text{Ca}^{2+}] \cdot \text{R}_\text{t} \tag{5}$$

$$[\text{nssSO}_4^{2-}] = [\text{SO}_4^{2-}] - \text{R}_\text{s} \cdot [ss\text{Na}^+] \tag{6}$$

with

$$R_m = (Na^+/Ca^{2+})_{ss}^{-1} \tag{7}$$

and

130 $$R_t = (Na^+/Ca^{2+})_{nss}, \tag{8}$$

where R_m and R_t are the Ca^{2+}:Na^+ sea-salt and continental ion mass ratios respectively and R_s is the sea salt ion mass ratio for SO_4^{2-}. Values of 1.78, 0.038 and 0.25 were used for R_m, R_t and R_s, respectively (Röthlisberger et al., 2002; Bigler et al., 2006). As described in Rowell et al. (2022), to make best use of the Ca^{2+} data while avoiding contaminated or missing data, the Ca^{2+} data points for the first sample in each drop of the drill (which is generally contaminated) were replaced with the mean of
135 the rest of the drop. This enables use of the Ca^{2+} record to obtain $ssNa^+$ and subsequently $nssSO_4^{2-}$ apportionments.

The concentrations of MSA, SO_4^{2-} and $nssSO_4^{2-}$ were plotted together (Figure 4), to identify potential volcanic peaks in the SO_4^{2-} record. MSA is used to corroborate the $nssSO_4^{2-}$ record, by providing a reference record of purely marine biogenic origin, to assist in the identification of $nssSO_4^{2-}$ peaks that are not related to fluctuations in marine inputs (Saigne and Legrand, 1987). Several eruptions known to leave a signal in the SO_4^{2-} records of multiple ice cores from across Antarctica were targeted in
140 particular. Specifically these events were: Tambora in 1815, an unidentified event from 1809, Kuwae in 1458 and the sequence of eruptions that occurred between 1230 – 1285, including Samalas in 1259 (Sigl et al., 2014). Multiple viable peaks, including some not related to these targeted events, were identified in approximately the expected depth regions for these events.

Sulfur (S) has four stable isotopes: ^{32}S, ^{33}S, ^{34}S, ^{36}S, which have natural relative abundances of 95.02%, 0.75%, 4.21% and 0.02%, respectively. Volcanic emissions have isotopically-light S compositions (i.e., relatively depleted in the ^{34}S isotope)
145 compared to other dominant inputs of SO_4^{2-} from marine biogenic emissions or sea salt (Rees et al., 1978; Nielsen et al., 1991; Patris et al., 2000; Crick et al., 2021). As such, the ^{34}S composition (reported relative to Vienna-Canyon Diablo Troilite in ‰, Equation 9) can be used to determine peaks in SO_4^{2-} that have a volcanic source. The relative difference between the $\delta^{34}S$ and $\delta^{33}S$ values and the ratio expected from equilibrium fractionation is expressed using $\Delta^{33}S$ notation (Equation 10, in ‰). Values of $\Delta^{33}S$ that are outside analytical error of zero show mass-independent fractionation (Farquhar et al., 2001). Mass-independent
150 fractionation of S isotopes occurs when sulfur dioxide gases are photo-oxidised to SO_4^{2-} by short-wave UV radiation (Savarino et al., 2003). This process only occurs above the ozone layer meaning non-zero $\Delta^{33}S$ values indicate volcanic eruptions where the eruptive plume reached the stratosphere (Gautier et al., 2019; Burke et al., 2019). Due to the relatively high background concentration of SO_4^{2-} in the SI:RAID samples, S isotope analysis was used to identify SO_4^{2-} peaks that have a volcanic source, which increases the confidence in identifying specific volcanic events in the SO_4^{2-} data.

155 $$\delta^x S = (\frac{(\delta^x S/\delta^{32}S)_{sample}}{(\delta^x S/\delta^{32}S)_{standard}} - 1) \times 1000 \tag{9}$$

where x is either ^{34}S or ^{33}S.
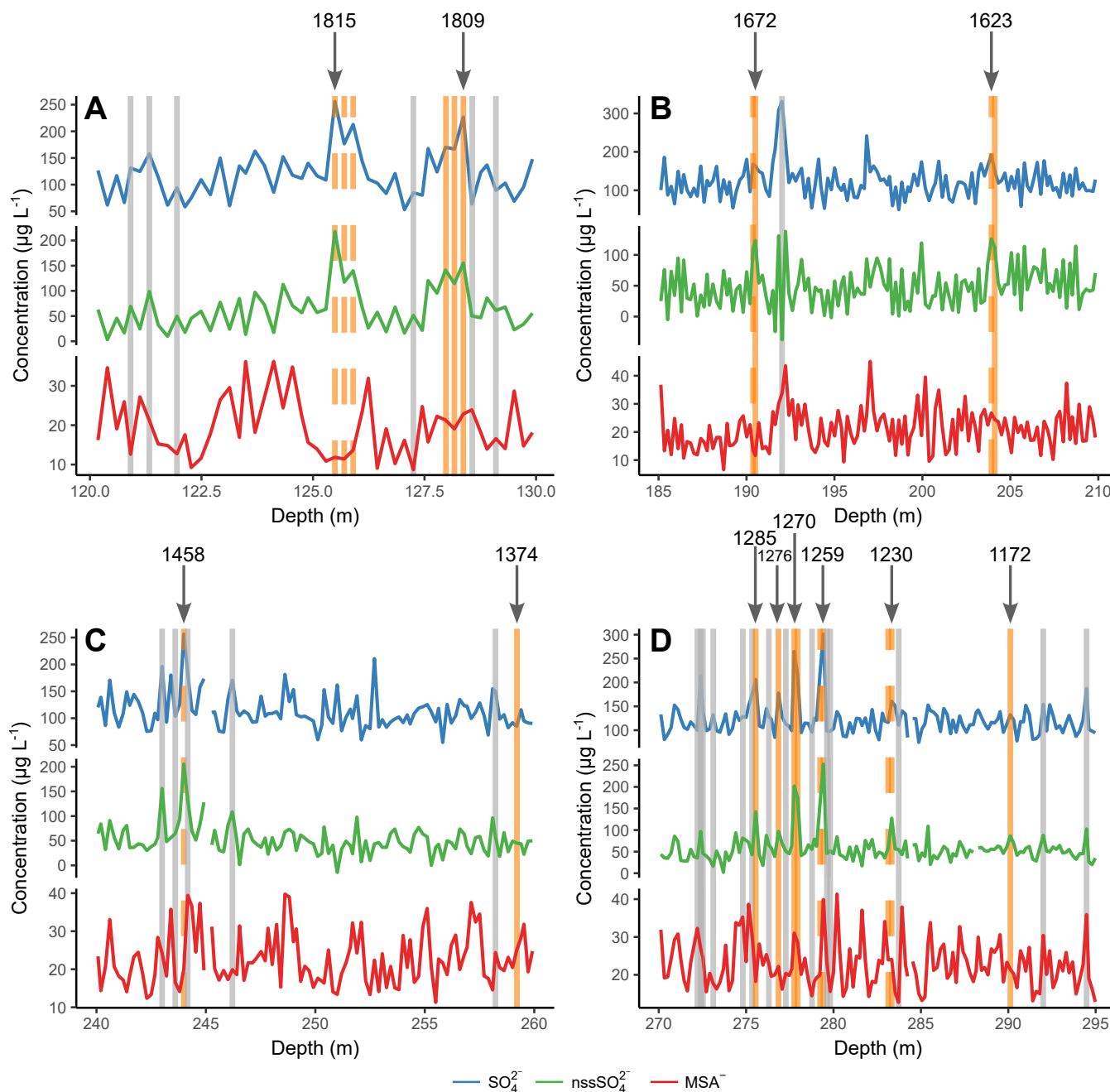
Figure 4. Identification of potential volcanic markers. The vertical lines show candidate peaks in the SO_4^{2-} record that were analysed for S isotope compositions. Grey lines show the depths of samples that had background, non-volcanic S isotope compositions, yellow lines show the depth of samples that had low $\delta^{34}S$ values, indicative of volcanically-derived SO_4^{2-} and dashed lines show volcanic peaks of stratospheric origin, defined by non-zero $\Delta^{33}S$ values. Panels A, B, C and D show the discrete depth ranges in which the identified volcanic markers appear. Arrows and numbers show the year of the identified event (CE).

$$\Delta^{33}S = \delta^{33}S - ((\delta^{34}S + 1)^{0.515} - 1) \times 1000 \qquad (10)$$

A total of 76 samples from Sherman Island were analysed for their S isotope composition, using the method described in (Hoffmann et al., 2022), and 12 individual volcanic eruptions were identified (Figure 4). All S isotope data for the identified

160 eruptions are provided in Table A1 and all individual sample S isotope data in the Supplement S1. Through a combination of comparison to the modelled age (Figure 5, Panel B), assessing the relative depth-age difference between eruptions and cross-checking against previously identified volcanic eruptions in Antarctic ice cores, the eruptions were dated. The SO_4^{2-} peaks are believed to correspond to the eruption of Tambora in 1815, an eruption of unknown origin in 1809, Kuwae in 1485, five eruptions of the thirteenth century (including Samalas) sequence (1285, 1276, 1270, 1259 and 1230), eruptions in 1623, 1672,

165 1372 and an eruption of unknown origin in 1172 (Sigl et al., 2014). Several eruptions were defined by multiple samples and show the evolution of δ^{34}S and Δ^{33}S values during an eruptive event. Samples that had non-volcanic S isotope values (δ^{34}S ranging from 15.95 to 20.33 ‰; mean = 18.17, n = 56) were also measured between every volcanic event to allow for precise depth assignment and ensure that multiple eruptions were defined by separate peaks. The 12 identified eruptions were all used for the final the age/depth interpolation as described below.

3.0.4 Model optimisation and final depth/age interpolation

The deepest fixed age marker attributable to a known volcanic event is at 290 m depth (year 1172 CE). To date the remaining 33 m of ice samples and remaining ice below the drilled depth, we use an depth/age model that assimilates age markers and optimises past accumulation and ice flow parameters.

The depth/age model is the result of an optimisation. We use a model that is identical to the one described in Section 3.0.2 but

175 we find the values of accumulation variation $a(t)$ that provide a best fit between the model and the age markers. For simplicity we assume that the accumulation rate history, $a(t)$, is a piece-wise linear function and that $2 < p < 3$. Under this assumptions we optimise the model using the Simplex method from Lagarias et al. (1998) as coded in the *fminsearch* function of *Matlab*.

The result of the depth/age model is shown, alongside the original model, in Figure 5 (Panel B). Due to the good agreement between the optimised model and the majority of the volcanic age markers, the age for the deepest sample at 323 m was

180 interpolated directly from the optimised depth/age model.

The age model can not be taken directly as the age scale for the full record, due to it not accurately capturing the volcanic tie points at 1815 and 1809. The model calculates these depths as 17 years younger (more recent). This is likely due to the actual accumulation history at the site being more variable than in the model, with a greater increase in accumulation between the 1458 eruption and the annual layer count end than is accounted for in the model. Two interpolation methods were carried

185 out between the annual counts, volcanic tie points and the age-model point for 323 m: a linear interpolation (for reference) and a Locally Estimated Scatter-Plot Smoothing (LOESS) method using multiple smoothing spans. The age scale computed using LOESS interpolation with span 0.05 fitted all known tie markers and was therefore chosen as the final age scale for the data.
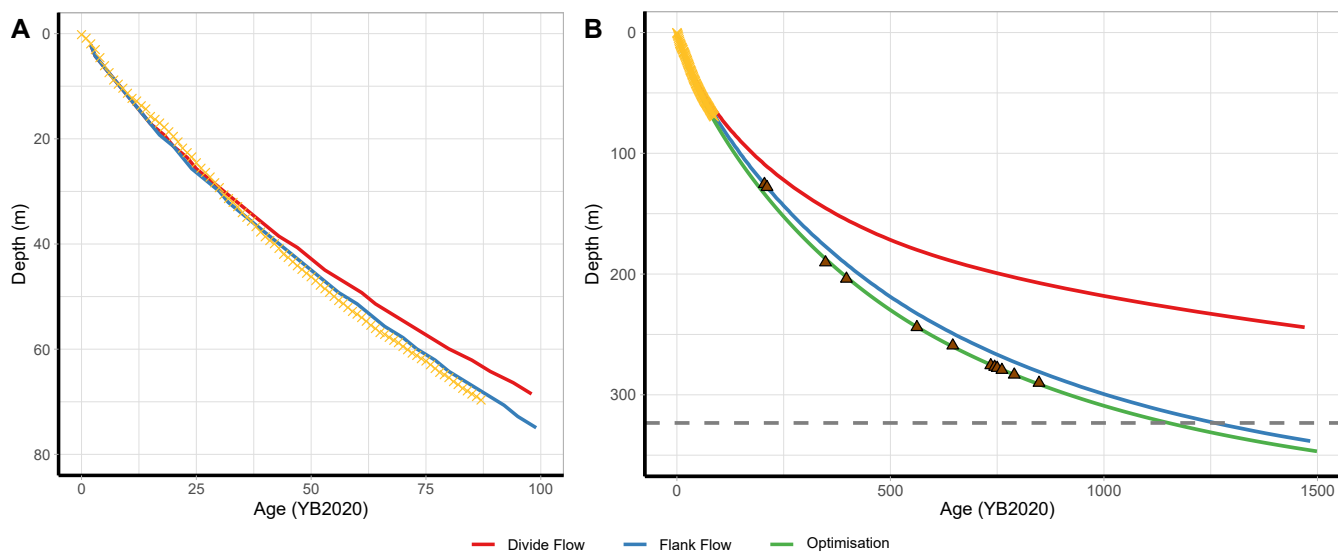
Figure 5. A: Original model, divide flow (red) and flank flow (blue), with annual layer counts (yellow crosses). B: original model flank and divide flows (red and blue lines) optimised model (green), with annual layer counts (yellow crosses) and volcanic tie markers (brown triangles). The grey dotted line shows the bottom of the borehole and drilled ice.

4 Final age scale

4.1 Age scale and uncertainty

190 The depth/age profile, with uncertainty limits, of the SI:RAID data is shown in Figure 6. Depths and ages presented represent the bottom of each sample, unless specified otherwise; the full age scale dataset with top and bottom depths and ages can be found in Supplement S2. The 323 m record of ice samples reach an age of 1082 years before 1950, or the year 868 CE, ± 29 years. The age profile follows closely to idealised glacial flow, with small adjustments in accumulation necessary to satisfactorily intercept every known age marker, as discussed below. The maximum absolute uncertainty in the whole record is

195 29 years at 323 m, a percentage uncertainty of 2.5% of the total age at that point.

An uncertainty estimate was calculated for the annual counts, each volcanic tie point, the mid-points between each tie point, and finally for the model interpolation point, as described below.

The uncertainty associated with the annual layer counting was estimated using the SI:RAID and SI:Core annual counts together to assess the presence or absence of uncertain annual layers. Peaks present in some species in RAID data were which were not identified in the Core (or vice versa, shown by yellow bars in Figure 2), indicate uncertain years. There were two

200 uncertain years out of 21 counted years for the top 21.8 m (when the SI:Core data ends), an uncertainty of 9.5 %. A 10 % uncertainty was therefore applied throughout the section that was annually counted in the RAID data (to 70 m).

For the volcanic tie points, we are confident about the identified volcanoes and their timing of eruption. Uncertainty at the tie point comes only from the depth interval of each eruption and its corresponding range of ages. Some of the identified
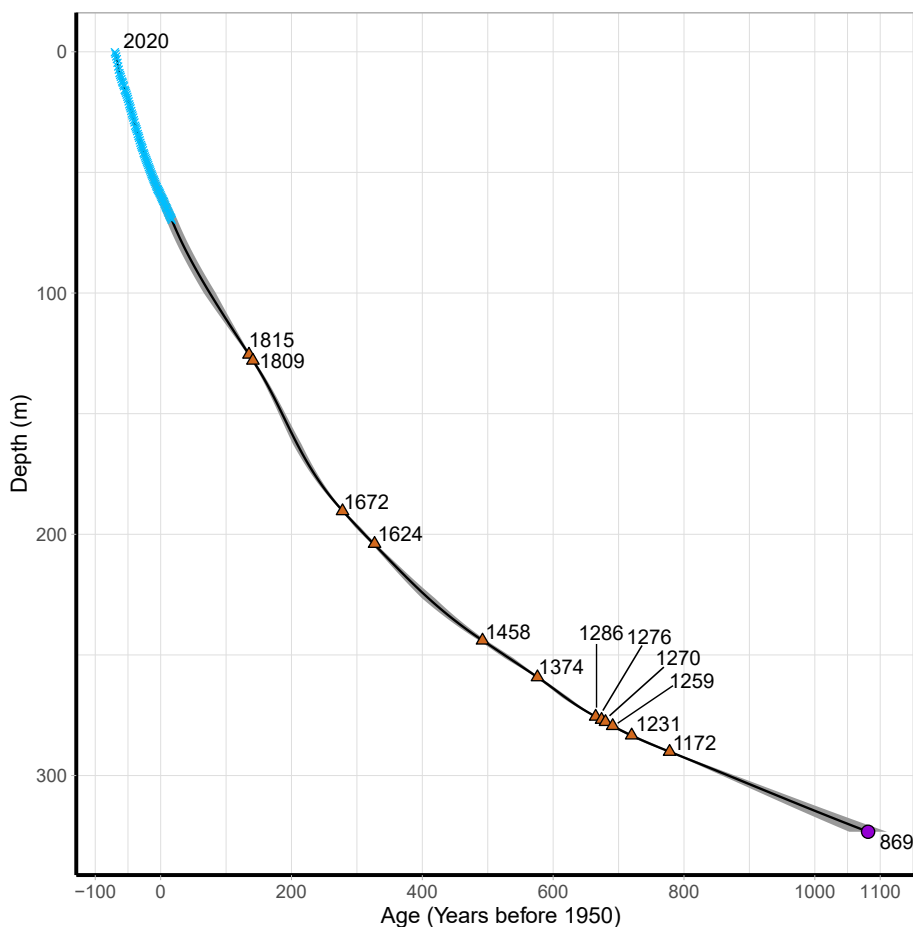
Figure 6. The final SI:RAID age scale (black line), shown with the respective age markers (blue crosses are annual layer counts, orange filled triangles are tie point volcanic events, purple circle is model interpolation) used in its development and grey shading indicating uncertainty.

205 volcanic events are recorded in the SO_4^{2-} record over multiple samples. When this was the case, the sample with the highest SO_4^{2-} concentration was chosen as the year of the event. Based on interpolation of the age scale to the point of each volcanic event, the age interval of that sample and surrounding samples was calculated. This gives an uncertainty for each volcanic tie point.

  Generally the tie points lie on a smooth line (Figure 6), suggesting that the offset of points between ties from the line is likely
210 to be small. However, the offset of the 1815/1809 pair from the smooth line, of 17 years, at a point that is approximately 130 years from the nearest other tie points suggests that a conservative estimate of the uncertainty between ties could be as high as 13 % of the distance from a tie point. We therefore estimated the uncertainty between ties as 13 % of the distance from the nearest tie point, added to the average uncertainty at the two adjacent ties (2).

Table 2. Estimates of age uncertainty for every tie point used in the SI:RAID age scale interpolation and the mid points between them (to nearest sample). Ages given in Year CE rounded to nearest year.

Tie point type	Sample(s)	Bottom Depth (m)	Sample Bottom Age (CE)	Total uncertainty (years)
Top	1	0	0	0
Annual layer count bottom	366	69.70	1933	8.5
Mid point	532	99.87	1875	9.2
1815 Eruption	668	125.49	1815	2.0
1809 Eruption	682	128.17	1809	2.1
Mid point	865	162.71	1741	6.5
1672 Eruption	1014	190.37	1672	2.0
Mid point	1051	197.22	1648	4.2
1624 Eruption	1087	203.92	1624	3.4
Mid point	1207	226.52	1541	9.9
1458 Eruption	1301	243.99	1458	5.6
Mid point	1341	251.40	1417	6.8
1374 Eruption	1383	259.20	1374	2.9
Mid point	1428	267.52	1332	5.2
1286 Eruption	1471	275.55	1285	1.8
Mid point	1473	275.96	1282	2.0
1276 Eruption	1478	276.85	1276	1.7
Mid point	1480	277.27	1273	2.2
1270 Eruption	1483	277.75	1270	2.3
Mid point	1487	278.56	1265	2.8
1259 Volcano	1492	279.42	1259	2.6
Mid point	1503	281.50	1245	4.4
1231 Eruption	1513	283.33	1231	4.3
Mid point	1533	286.83	1202	5.1
1172 Eruption	1551	290.11	1172	2.1
Model	1552 to 1726	290.31 to 323.3	868 to 1170	2.3 to 28.8

The difference between the modelled and empirically derived age scale was calculated for every tie point based on the
215 annual layer counting and volcanic horizon identification. Using these differences, the maximum percentage deviation from the modelled age was chosen and applied to the samples below the final tie point, to give an uncertainty for the bottom of the core. By selecting the maximum percentage deviation this allows a conservative estimate of the uncertainty, erring on the side of larger error.

The age scale uncertainty was interpolated to every sample using a linear interpolation of the error between the points shown
220 in Table 2, up to the last tie point (volcanic at 1172 CE). For all samples below this depth, the maximum model uncertainty (8.8%) was applied as a percentage relative to the age difference from the final tie point (1172 CE), added to the uncertainty at that tie point. All uncertainty values are shown in Table 2.

4.2 Prediction of age near the bedrock

Predicting the age of the 105 m of ice below the bottom sample depth, where the drill was lost, is more uncertain. The model
225 was used to estimate the age of the ice towards the bed at the RAID drilling site, however in the lowest 13 metres, model
outputs are meaningless. This is because in our depth/age model we assume no basal melting and the solution to Equation
1 is that the age of ice at the bottom tends to infinity. Numerically this translates into a solution at the bottom that depends
on the numerical details used as grid and time step size or initial conditions. Instead, we use as a conservative indication of
the maximum expected age the age at 90% depth (385.2 m). The flank age of the non-optimised model predicts an age of
230 2677 ± 230 years before 1950 (Figure 7, range estimated from the span of ages resulting from accumulation rates of 0.68 to
0.76). We discuss the longest possible record attainable from the site in Section 5.4 below. Assuming no significant change in
accumulation - the modelled (optimised) change in accumulation is only 4 % for the existing samples - it is likely that a record
covering the majority of the Holocene is achievable from Sherman Island (darker lines in Figure 7). Our expectation is that the
depth of older features, such as the Last Glacial Maximum (LGM), if present, are likely on the order of a maximum of a few
235 metres above the bed.

4.3 Seasonality of chemical species

The species used for annual layer counting were interpolated to monthly resolution for their entire records. Monthly mean
anomaly concentrations, relative to annual means, were then calculated to investigate the seasonality of species with depth,
using methods similar to Hoffmann et al. (2022) (Figure 8). All species show strong seasonality in the top 20 years, which
240 were annually counted alongside SI:Core. SO_4^{2-} and $\delta^{18}O$ demonstrate this continued seasonality consistently to 70 m (annually
counted). MSA^- also demonstrates a seasonal pattern throughout this period, but with a changed seasonality from a summer
peak to a slight winter peak, in line with Na^+. This migration of the MSA^- peak has been well documented in ice cores (Osman
et al., 2017), and in the SI:RAID samples begins at approximately 30 m, with inconsistent peaks for 15 m followed by consistent
winter peaks by 46 m depth.

245 # 5 Discussion

5.1 Annual layer counting

The Sherman Island RAID samples present a relatively low resolution ice core record due to the sampling restraints to keep
cargo minimal. The samples average 19 cm depth resolution, in age increments ranging from 0.04 to 2.38 years with an
average of 0.7 years. This presents a challenge for dating compared to other ice cores; traditional ice cores can be sampled and
250 measured at any chosen resolution, typically on the order of a few cm for continuous flow analyses in shallow to intermediate
depth cores (e.g., Tetzner et al. (2021); Grieman et al. (2022)). Considering this limitation, the ice from Sherman Island has
been dated relatively robustly from a combination of approaches widely used in ice core analysis, but adjusted to allow for
the unique SI:RAID samples. For example, annual layer counting was only possible to a relatively shallow depth (70 m, 85
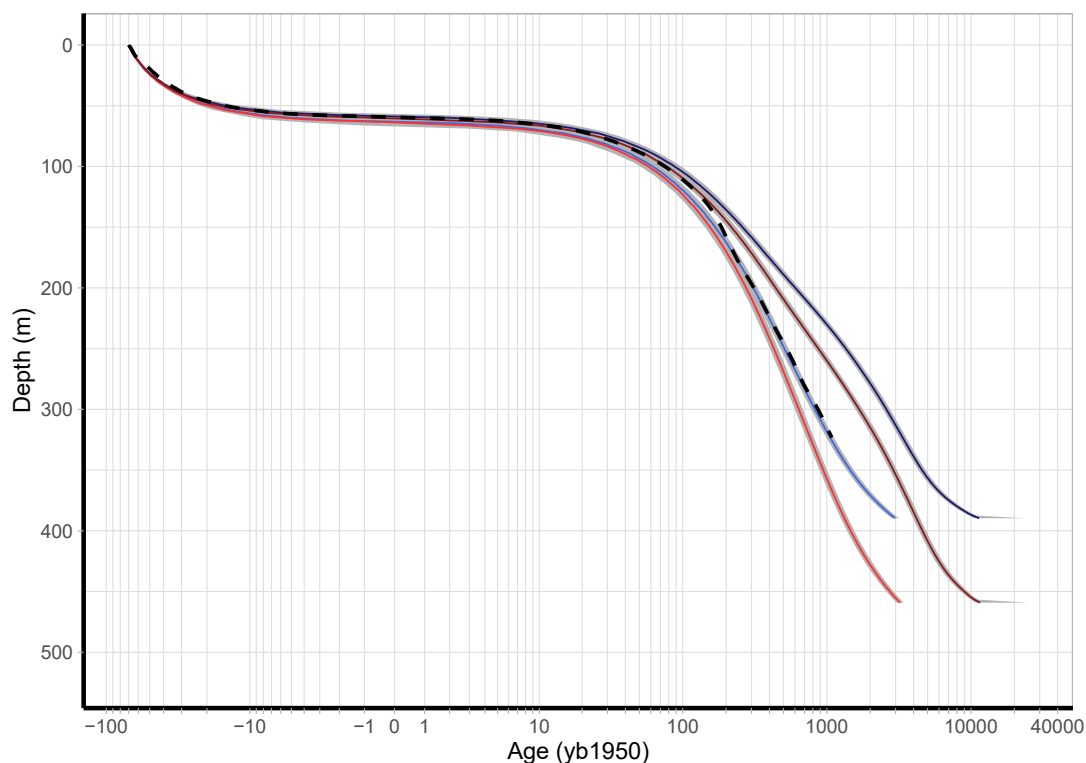
Figure 7. Ice thinning model predictions of ice age at 90 % depth at RAID drilling location (blue lines) for divide (dark blue) and flank (light blue) flow regimes, and at the deepest point of Sherman Island (red lines) for divide (dark red) and flank (light red) flow regimes. The dashed black line shows the actual age scale of the SI:RAID samples. Grey shading shows upper and lower estimates based on a range of accumulation rate values supplied to the thinning model, which were in turn based on the best fitting calculated present accumulation from the optimisation model, run at 3 flow regimes, p = 2 to 4 (Equation 3).

years). In comparison, WAIS Divide and Skytrain ice cores are annually dated to 31.2 ka BP (2850 m) and 1942 years BP
255 (184.14 m), respectively (Sigl et al., 2016; Hoffmann et al., 2022). Annual layer counting was aided by comparison with a short but very proximal ice core, sampled on a higher resolution; the SI:Core was sampled at 5 cm resolution compared with the average of 18 cm for the corresponding depth range of SI:RAID. The existence of such a close ice core for comparison and to assist the dating strategy is not a common occurrence in deep ice core drilling. This proximity is valuable because two such closely located ice cores should not have age scales which significantly deviate from each other, due to experiencing similar
260 accumulation histories.

5.2 Volcanic horizon identification

Volcanic synchronisation of ice core records and dating of individual ice cores using volcanic event identification using the
SO_4^{2-} data of cores is a standard ice core dating technique (e.g., Fujita et al. (2015); Narcisi et al. (2006); Palmer et al. (2001);
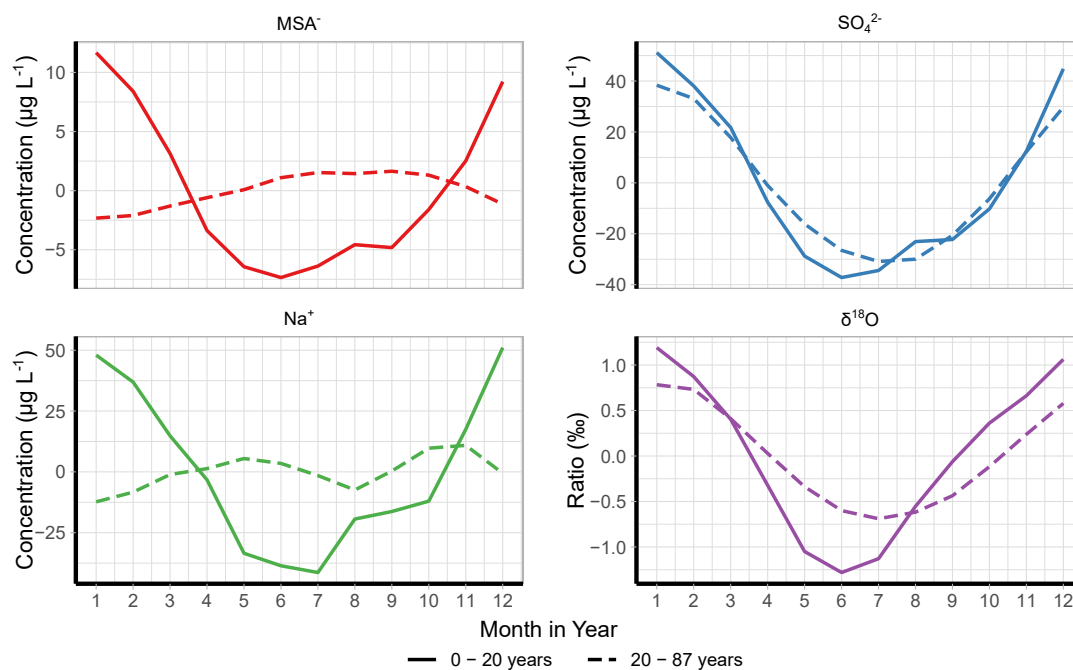
Figure 8. Seasonality of certain chemical species and stable water isotope composition. The x-axes shows month of the year (1 is January and 12 is December) and the y-axes show anomaly concentrations or composition of the species, relative to the annual mean. Line types are for shallow dated section (0 to 20 m) and annual layer counted section (20 to 70 m).

Severi et al. (2017), and others). In this case, SO_4^{2-} peak identification was supplemented with S-isotope analysis, giving more
265 confidence that: first, some of the SO_4^{2-} peaks identified were of volcanic origin and second, that their isotopic characteristics matched those of the expected volcanic eruption being used to assign an age horizon for its respective depth. Being confident in the eruptions identified meant that the uncertainty of those age horizons was effectively zero, being equivalent only to the estimated age increment covered by the sample depth due to the necessarily low sampling resolution.

5.3 Modelling

270 Finally, the use of an ice thinning model that allows accumulation to vary in order to fit through empirical tie points resulted in a more realistic estimate of the age-depth relationship. This model also enabled the interpolation of an age estimate for the bottom-most sample, which would have been difficult to date in any other way, allowing an age scale for the full range of SI:RAID samples to be developed. The model also helped to calculate the age scale uncertainty. Further use of the model is discussed below.

5.4 Deepest ice: Is it possible to find a continuous record beyond the Holocene in Sherman Island?

Is it possible to find a continuous record beyond the Holocene in Sherman Island? To answer that question, we discuss here the influence of local ice flow on depth/age. Beyond the modelling details, the ice flow near a ridge can be characterised by the proximity to the divide of flow, the vertical plane where ice starts flowing towards the opposite flanks of the ridge that is often located near the ridge. This is a result of ice having a non-linear rheology (Raymond, 1983). Some distance from the divide, only a few ice thicknesses, flow is dominated by shear and it is well represented by the Lliboutry approximation with a parameter p larger than 1. At the divide, however, the lower strain-rates near the bed and the non-linearity of ice translate into nearly stagnant ice. These local flow conditions have a strong influence on depth/age, as shown in Figure 5.

Intriguingly, as we mentioned earlier, it is clear that the depth/age at SI:RAID only fits the flanking flow model and, under no reasonable assumptions of past accumulation, the divide flow model is able to fit the observed age markers. However, if we were to find a site in Sherman Island at a divide of flow, our model estimates that, assuming identical accumulation history, the age-depth at 90% depth is 9427 ± 500 years before 1950 (Figure 7).

There is a hint from IceBridge data over the ridge near our drilling location (IRMCR1B_20181116_02_020) that such flow conditions could exist on the opposite side of the ridge from our drilling site. This is because the low-strain rates near the base at the divide flow manifest conspicuously as arches in the ice structure (Vaughan et al., 1999). The radargram, however, is not clear due to the strong slopes in the radar layers induced by the divide conditions and we recommend further geophysical survey.

Another potential drilling site on the island is near the summit, where ice is thicker. Near the summit, ice is approximately 80 m deeper than the SI:RAID site. Our model estimates that, assuming identical accumulation history, under divide flow conditions the age at 90 % depth (459 m) is 10700 to 23650 years before 1950 and under flank flow 3200 ± 200 years before 1950 (Figure 7).

6 Conclusions

An age scale for the SI:RAID samples, which extends back to more than 1150 years before present day and is currently the longest ice core from the coastal West Antarctic and western Antarctic Peninsula regions, has been presented. The use of IC and S-isotope measurements on RAID-drilled ice to establish an age scale is presented here for the first time, in addition to stable water isotopic measurements. The SI:RAID data will make a valuable contribution to regional, continental and global compilation projects such as PAGES-2k (PAGES 2k Coordinators, 2017). There is a lack of a recent Antarctic Holocene ice core composite, and the 1000 years of climate data from Sherman Island could make a significant contribution to work such as this (Masson et al., 2000). If in the future a full scale drilling campaign on Sherman Island were to be carried out, a longer, full Holocene record for this region in West Antarctica could probably be obtained by drilling to bedrock at the deepest point of Sherman Island. Such a record would be critical in gaining insights into West Antarctic interglacial variability. The records contained in the existing SI data have the potential to constrain the last 1000 years of climate history in this important and vulnerable region of West Antarctica and represent a valuable addition to the ice core community.

Table A1. All S isotope data from the identified volcanic eruptions in the SI:RAID samples. Samples 683 and 1015 were analysed before a reliable Δ^{33}S method had been developed and Δ^{33}S data therefore does not exist for these samples.

Sample	Depth (m)	δ^{34}SO$_4$ (‰)	Δ^{33}S (‰)	Volcanic?	Stratospheric?	Year
668	125.49	2.67	-0.38	Volcanic	Yes	1815
669	125.70	8.66	0.05	Volcanic	Yes	1815
670	125.90	16.17	0.77	Volcanic	Yes	1815
681	127.97	10.26	-0.04	Volcanic	No	1809
682	128.17	9.39	0.04	Volcanic	No	1809
683	128.37	15.20	N/A	Volcanic	Unknown	1809
1014	190.37	12.71	-0.16	Volcanic	Yes	1672
1015	190.50	10.06	N/A	Volcanic	Unknown	1672
1087	203.92	15.84	-0.40	Uncertain	Yes	1624
1088	204.11	14.48	0.09	Uncertain	Uncertain	1624
1301	243.99	7.43	-0.17	Volcanic	Yes	1458
1383	259.20	11.37	-0.01	Volcanic	No	1374
1471	275.55	12.31	-0.10	Volcanic	Uncertain	1286
1478	276.85	13.90	-0.02	Volcanic	No	1276
1483	277.75	11.05	0.02	Volcanic	No	1270
1484	277.95	9.38	0.04	Volcanic	No	1270
1491	279.22	0.20	-0.78	Volcanic	Yes	1259
1492	279.42	13.76	0.40	Volcanic	Yes	1259
1512	283.13	16.18	-0.18	Volcanic	Yes	1231
1513	283.33	8.56	-0.43	Volcanic	Yes	1231
1551	290.11	15.38	-0.02	Uncertain	No	1172

Author contributions. The manuscript was written by IR with contributions from CM, HP, EW, and DT. The RAID ice was drilled and sampled by RM, IR and DT. The SI ice core was drilled by DT. The RAID samples were analysed by IR. The SI ice core was processed and analysed and data made available for use by DT. The sulfur isotope analysis was done by HP and ED. The annual layer counting was done by IR, with ice core contributions from DT. The volcanic horizon identification was done by IR, HP and EW. The models were developed by CM and used by IR with assistance from CM. The age scale uncertainty estimation was done by IR with assistance from EW and CM. The seasonality analysis was done by IR. Age predictions were done by IR, CM and EW.

310

Competing interests. The authors wish to declare that Eric Wolff, one of the co-authors of this manuscript, is a member of the editorial board for Climate of the Past.

315

Acknowledgements. This project has received funding from the European Research Council under the Horizon 2020 research and innovation programme (grant agreement No 742224, WACSWAIN). This material reflects only the author's views and the Commission is not liable for any use that may be made of the information contained therein. EW has also been funded through a Royal Society Professorship.

The drilling of the Sherman Island shallow ice core was supported by the Collaborative Antarctic Science Scheme (CASS-168). Data obtained from the Sherman Island shallow ice core was funded by a CONICYT–Becas Chile and Cambridge Trust fellowship awarded to Dieter Tetzner, grant number 72180432.

The authors would like to thank Shaun Miller and Jack Humby for their assistance with the lab analyses necessary for this project.

References

Bamber, J. L., Oppenheimer, M., Kopp, R. E., Aspinall, W. P., and Cooke, R. M.: Ice sheet contributions to future sea-level rise from struc-
325   tured expert judgment, Proceedings of the National Academy of Sciences, 116, 11 195–11 200, https://doi.org/10.1073/pnas.1817205116,
publisher: Proceedings of the National Academy of Sciences, 2019.

Bazin, L., Landais, A., Lemieux-Dudon, B., Toyé Mahamadou Kele, H., Veres, D., Parrenin, F., Martinerie, P., Ritz, C., Capron, E., Lipenkov,
V., Loutre, M.-F., Raynaud, D., Vinther, B., Svensson, A., Rasmussen, S. O., Severi, M., Blunier, T., Leuenberger, M., Fischer, H., Masson-
Delmotte, V., Chappellaz, J., and Wolff, E.: An optimized multi-proxy, multi-site Antarctic ice and gas orbital chronology (AICC2012):
330   120–800 ka, Climate of the Past Discussions, 8, 5963–6009, https://doi.org/10.5194/cpd-8-5963-2012, 2012.

Bigler, M., Röthlisberger, R., Lambert, F., Stocker, T. F., and Wagenbach, D.: Aerosol deposited in East Antarctica over the last
glacial cycle: Detailed apportionment of continental and sea-salt contributions, Journal of Geophysical Research: Atmospheres, 111,
https://doi.org/10.1029/2005JD006469, 2006.

Bronselaer, B., Winton, M., Griffies, S. M., Hurlin, W. J., Rodgers, K. B., Sergienko, O. V., Stouffer, R. J., and Russell, J. L.: Change
335   in future climate due to Antarctic meltwater, Nature, 564, 53–58, https://doi.org/10.1038/s41586-018-0712-z, number: 7734 Publisher:
Nature Publishing Group, 2018.

Burke, A., Moore, K. A., Sigl, M., Nita, D. C., McConnell, J. R., and Adkins, J. F.: Stratospheric eruptions from tropical and extra-
tropical volcanoes constrained using high-resolution sulfur isotopes in ice cores, Earth and Planetary Science Letters, 521, 113–119,
https://doi.org/10.1016/j.epsl.2019.06.006, 2019.

340 Crick, L., Burke, A., Hutchison, W., Kohno, M., Moore, K. A., Savarino, J., Doyle, E. A., Mahony, S., Kipfstuhl, S., Rae, J. W. B., Steele,
R. C. J., Sparks, R. S. J., and Wolff, E. W.: New insights into the ~74 ka Toba eruption from sulfur isotopes of polar ice cores, preprint,
Atmospheric Dynamics/Ice Cores/Pleistocene, https://doi.org/10.5194/cp-2021-38, 2021.

DeConto, R. M. and Pollard, D.: Contribution of Antarctica to past and future sea-level rise, Nature, 531, 591–597,
https://doi.org/10.1038/nature17145, 2016.

345 Delmas, R. J., Legrand, M., Aristarain, A. J., and Zanolini, F.: Volcanic deposits in Antarctic snow and ice, Jour-
nal of Geophysical Research: Atmospheres, 90, 12 901–12 920, https://doi.org/10.1029/JD090iD07p12901, _eprint:
https://onlinelibrary.wiley.com/doi/pdf/10.1029/JD090iD07p12901, 1985.

Edwards, T. L., Brandon, M. A., Durand, G., Edwards, N. R., Golledge, N. R., Holden, P. B., Nias, I. J., Payne, A. J., Ritz, C., and Wer-
necke, A.: Revisiting Antarctic ice loss due to marine ice-cliff instability, Nature, 566, 58–64, https://doi.org/10.1038/s41586-019-0901-4,
350   number: 7742 Publisher: Nature Publishing Group, 2019.

Farquhar, J., Savarino, J., Airieau, S., and Thiemens, M. H.: Observation of wavelength-sensitive mass-independent sulfur isotope ef-
fects during SO2 photolysis: Implications for the early atmosphere, Journal of Geophysical Research: Planets, 106, 32 829–32 839,
https://doi.org/10.1029/2000JE001437, _eprint: https://onlinelibrary.wiley.com/doi/pdf/10.1029/2000JE001437, 2001.

Fujita, S., Parrenin, F., Severi, M., Motoyama, H., and Wolff, E. W.: Volcanic synchronization of Dome Fuji and Dome C Antarctic deep ice
355   cores over the past 216 kyr, Climate of the Past, 11, 1395–1416, https://doi.org/10.5194/cp-11-1395-2015, 2015.

Gautier, E., Savarino, J., Hoek, J., Erbland, J., Caillon, N., Hattori, S., Yoshida, N., Albalat, E., Albarede, F., and Farquhar, J.: 2600-years of
stratospheric volcanism through sulfate isotopes, Nature Communications, 10, 466, https://doi.org/10.1038/s41467-019-08357-0, 2019.

Grieman, M. M., Hoffmann, H. M., Humby, J. D., Mulvaney, R., Nehrbass-Ahles, C., Rix, J., Thomas, E. R., Tuckwell, R., and Wolff, E. W.: Continuous flow analysis methods for sodium, magnesium and calcium detection in the Skytrain ice core, Journal of Glaciology, 68, 90–100, https://doi.org/10.1017/jog.2021.75, tex.ids= grieman_continuous_2022 publisher: Cambridge University Press, 2022.

Hoffmann, H. M., Grieman, M. M., King, A. C. F., Epifanio, J. A., Martin, K., Vladimirova, D., Pryer, H. V., Doyle, E., Schmidt, A., Humby, J. D., Rowell, I. F., Nehrbass-Ahles, C., Thomas, E. R., Mulvaney, R., and Wolff, E. W.: The ST22 chronology for the Skytrain Ice Rise ice core – Part 1: A stratigraphic chronology of the last 2000 years, Climate of the Past, 18, 1831–1847, https://doi.org/10.5194/cp-18-1831-2022, publisher: Copernicus GmbH, 2022.

Joughin, I. and Alley, R. B.: Stability of the West Antarctic ice sheet in a warming world, Nature Geoscience, 4, 506–513, https://doi.org/10.1038/ngeo1194, 2011.

Konrad, H., Shepherd, A., Gilbert, L., Hogg, A. E., McMillan, M., Muir, A., and Slater, T.: Net retreat of Antarctic glacier grounding lines, Nature Geoscience, 11, 258–262, https://doi.org/10.1038/s41561-018-0082-z, number: 4 Publisher: Nature Publishing Group, 2018.

Lagarias, J. C., Reeds, J. A., Wright, M. H., and Wright, P. E.: Convergence Properties of the Nelder–Mead Simplex Method in Low Dimensions | SIAM Journal on Optimization, 9, 112–147, https://doi.org/10.1137/S1052623496303470, 1998.

Lenton, T. M., Held, H., Kriegler, E., Hall, J. W., Lucht, W., Rahmstorf, S., and Schellnhuber, H. J.: Tipping elements in the Earth's climate system, Proceedings of the National Academy of Sciences, 105, 1786–1793, https://doi.org/10.1073/pnas.0705414105, publisher: Proceedings of the National Academy of Sciences, 2008.

Lliboutry, L.: A Critical Review of Analytical Approximate Solutions for Steady State Velocities and Temperature in Cold Ice-sheets, google-Books-ID: jXFRtwAACAAJ, 1979.

Lowry, D. P., Krapp, M., Golledge, N. R., and Alevropoulos-Borrill, A.: The influence of emissions scenarios on future Antarctic ice loss is unlikely to emerge this century, Communications Earth & Environment, 2, 1–14, https://doi.org/10.1038/s43247-021-00289-2, number: 1 Publisher: Nature Publishing Group, 2021.

Martín, C. and Gudmundsson, G. H.: Effects of nonlinear rheology, temperature and anisotropy on the relationship between age and depth at ice divides, The Cryosphere, 6, 1221–1229, https://doi.org/10.5194/tc-6-1221-2012, publisher: Copernicus GmbH, 2012.

Martín, C., Mulvaney, R., Gudmundsson, G. H., and Corr, H.: Inferring palaeo-accumulation records from ice-core data by an adjoint-based method: application to James Ross Island's ice core, Climate of the Past, 11, 547–557, https://doi.org/10.5194/cp-11-547-2015, publisher: Copernicus GmbH, 2015.

Masson, V., Vimeux, F., Jouzel, J., Morgan, V., Delmotte, M., Ciais, P., Hammer, C., Johnsen, S., Lipenkov, V. Y., Mosley-Thompson, E., Petit, J. R., Steig, E. J., Stievenard, M., and Vaikmae, R.: Holocene climate variability in Antarctica based on 11 ice-core isotopic records, Quaternary Research, 54, 348–358, https://doi.org/10.1006/qres.2000.2172, 2000.

Matsuoka, K., Skoglund, A., Roth, G., de Pomereu, J., Griffiths, H., Headland, R., Herried, B., Katsumata, K., Le Brocq, A., Licht, K., Morgan, F., Neff, P. D., Ritz, C., Scheinert, M., Tamura, T., Van de Putte, A., van den Broeke, M., von Deschwanden, A., Deschamps-Berger, C., Van Liefferinge, B., Tronstad, S., and Melvær, Y.: Quantarctica, an integrated mapping environment for Antarctica, the Southern Ocean, and sub-Antarctic islands, Environmental Modelling & Software, 140, 105 015, https://doi.org/10.1016/j.envsoft.2021.105015, tex.ids= matsuoka_quantarctica_2021, 2021.

Mercer, J.: West Antarctic Ice Sheet and Co2 Greenhouse Effect - Threat of Disaster, Nature, 271, 321–325, https://doi.org/10.1038/271321a0, 1978.

Mulvaney, R., Rix, J., Polfrey, S., Grieman, M., Martìn, C., Nehrbass-Ahles, C., Rowell, I., Tuckwell, R., and Wolff, E.: Ice drilling on
  Skytrain Ice Rise and Sherman Island, Antarctica, Annals of Glaciology, pp. 1–13, https://doi.org/10.1017/aog.2021.7, tex.ids= mul-
  vaney_ice_2021 publisher: Cambridge University Press, 2021.

Narcisi, B., Robert Petit, J., and Tiepolo, M.: A volcanic marker (92ka) for dating deep east Antarctic ice cores, Quaternary Science Reviews,
  25, 2682–2687, https://doi.org/10.1016/j.quascirev.2006.07.009, 2006.

Nielsen, H., Pilot, J., Grinenko, L., Grinenko, V., Lein, A., Smith, J., and Pankina, R.: Lithospheric sources of sulphur, John Wiley and Sons,
  United Kingdom, iNIS Reference Number: 24035511, 1991.

Oppenheimer, M.: Global warming and the stability of the West Antarctic Ice Sheet, Nature, 393, 325–332, https://doi.org/10.1038/30661,
  1998.

Osman, M., Das, S. B., Marchal, O., and Evans, M. J.: Methanesulfonic acid (MSA) migration in polar ice: data synthesis and theory, The
  Cryosphere, 11, 2439–2462, https://doi.org/10.5194/tc-11-2439-2017, 2017.

PAGES 2k Coordinators: The third phase of the PAGES 2k Network, Past Global Changes Magazine, 25, 71–74,
  https://doi.org/10.22498/pages.25.1.71, 2017.

Palmer, A. S., Ommen, T. D. v., Curran, M. A. J., Morgan, V., Souney, J. M., and Mayewski, P. A.: High-precision dating of volcanic events
  (A.D. 1301–1995) using ice cores from Law Dome, Antarctica, Journal of Geophysical Research: Atmospheres, 106, 28 089–28 095,
  https://doi.org/10.1029/2001JD000330, 2001.

Paolo, F. S., Fricker, H. A., and Padman, L.: Volume loss from Antarctic ice shelves is accelerating, Science, 348, 327–331,
  https://doi.org/10.1126/science.aaa0940, publisher: American Association for the Advancement of Science, 2015.

Parrenin, F., Petit, J.-R., Masson-Delmotte, V., Wolff, E., Basile-Doelsch, I., Jouzel, J., Lipenkov, V., Rasmussen, S. O., Schwander, J., Severi,
  M., Udisti, R., Veres, D., and Vinther, B. M.: Volcanic synchronisation between the EPICA Dome C and Vostok ice cores (Antarctica)
  0-145 kyr BP, Climate of the Past, 8, 1031–1045, https://doi.org/10.5194/cp-8-1031-2012, 2012.

Patris, N., Delmas, R. J., and Jouzel, J.: Isotopic signatures of sulfur in shallow Antarctic ice cores, Jour-
  nal of Geophysical Research: Atmospheres, 105, 7071–7078, https://doi.org/10.1029/1999JD900974, _eprint:
  https://onlinelibrary.wiley.com/doi/pdf/10.1029/1999JD900974, 2000.

Pattyn, F. and Morlighem, M.: The uncertain future of the Antarctic Ice Sheet, Science, 367, 1331–1335,
  https://doi.org/10.1126/science.aaz5487, publisher: American Association for the Advancement of Science, 2020.

Rasmussen, S. O., Abbott, P. M., Blunier, T., Bourne, A. J., Brook, E., Buchardt, S. L., Buizert, C., Chappellaz, J., Clausen, H. B., Cook, E.,
  Dahl-Jensen, D., Davies, S. M., Guillevic, M., Kipfstuhl, S., Laepple, T., Seierstad, I. K., Severinghaus, J. P., Steffensen, J. P., Stowasser,
  C., Svensson, A., Vallelonga, P., Vinther, B. M., Wilhelms, F., and Winstrup, M.: A first chronology for the North Greenland Eemian Ice
  Drilling (NEEM) ice core, Climate of the Past, 9, 2713–2730, https://doi.org/10.5194/cp-9-2713-2013, 2013.

Raymond, C. F.: Deformation in the Vicinity of Ice Divides, Journal of Glaciology, 29, 357–373,
  https://doi.org/10.3189/S0022143000030288, publisher: Cambridge University Press, 1983.

Rees, C. E., Jenkins, W. J., and Monster, J.: The sulphur isotopic composition of ocean water sulphate, Geochimica et Cosmochimica Acta,
  42, 377–381, https://doi.org/10.1016/0016-7037(78)90268-5, 1978.

Rix, J., Mulvaney, R., Hong, J., and Ashurst, D.: Development of the British Antarctic Survey Rapid Access Isotope Drill, Journal of
  Glaciology, 65, 288–298, https://doi.org/10.1017/jog.2019.9, 2019.

Rowell, I. F., Mulvaney, R., Rix, J., Tetzner, D. R., and Wolff, E. W.: Viability of chemical and water isotope ratio measurements of RAID
  ice chippings from Antarctica, Journal of Glaciology, pp. 1–16, https://doi.org/10.1017/jog.2022.94, 2022.

Röthlisberger, R., Mulvaney, R., Wolff, E. W., Hutterli, M. A., Bigler, M., Sommer, S., and Jouzel, J.: Dust and sea salt variability in central East Antarctica (Dome C) over the last 45 kyrs and its implications for southern high-latitude climate, Geophysical Research Letters, 29, 1963, https://doi.org/10.1029/2002GL015186, 2002.

435 Saigne, C. and Legrand, M.: Measurements of methanesulphonic acid in Antarctic ice, Nature, 330, 240–242, https://doi.org/10.1038/330240a0, number: 6145 Publisher: Nature Publishing Group, 1987.

Savarino, J., Romero, A., Cole-Dai, J., Bekki, S., and Thiemens, M. H.: UV induced mass-independent sulfur isotope fractionation in stratospheric volcanic sulfate, Geophysical Research Letters, 30, https://doi.org/10.1029/2003GL018134, _eprint: https://onlinelibrary.wiley.com/doi/pdf/10.1029/2003GL018134, 2003.

440 Severi, M., Udisti, R., Becagli, S., Stenni, B., and Traversi, R.: Volcanic synchronisation of the EPICA-DC and TALDICE ice cores for the last 42 kyr BP, Climate of the Past, 8, 509–517, https://doi.org/10.5194/cp-8-509-2012, 2012.

Severi, M., Becagli, S., Caiazzo, L., Ciardini, V., Colizza, E., Giardi, F., Mezgec, K., Scarchilli, C., Stenni, B., Thomas, E. R., Traversi, R., and Udisti, R.: Sea salt sodium record from Talos Dome (East Antarctica) as a potential proxy of the Antarctic past sea ice extent, Chemosphere, 177, 266–274, https://doi.org/10.1016/j.chemosphere.2017.03.025, 2017.

445 Shepherd, A., Wingham, D., and Rignot, E.: Warm ocean is eroding West Antarctic Ice Sheet, Geophysical Research Letters, 31, https://doi.org/10.1029/2004GL021106, _eprint: https://onlinelibrary.wiley.com/doi/pdf/10.1029/2004GL021106, 2004.

Sigg, A. and Neftel, A.: Seasonal Variations in Hydrogen Peroxide in Polar Ice Cores, Annals of Glaciology, 10, 157–162, https://doi.org/10.3189/S0260305500004353, 1988.

Sigl, M., McConnell, J. R., Toohey, M., Curran, M., Das, S. B., Edwards, R., Isaksson, E., Kawamura, K., Kipfstuhl, S., Krüger, K., Layman, L., Maselli, O. J., Motizuki, Y., Motoyama, H., Pasteris, D. R., and Severi, M.: Insights from Antarctica on volcanic forcing during the Common Era, Nature Climate Change, 4, 693–697, https://doi.org/10.1038/nclimate2293, 2014.

Sigl, M., Fudge, T. J., Winstrup, M., Cole-Dai, J., Ferris, D., McConnell, J. R., Taylor, K. C., Welten, K. C., Woodruff, T. E., Adolphi, F., Bisiaux, M., Brook, E. J., Buizert, C., Caffee, M. W., Dunbar, N. W., Edwards, R., Geng, L., Iverson, N., Koffman, B., Layman, L., Maselli, O. J., McGwire, K., Muscheler, R., Nishiizumi, K., Pasteris, D. R., Rhodes, R. H., and Sowers, T. A.: The WAIS Divide deep ice core WD2014 chronology - Part 2: Annual-layer counting (0-31 ka BP), Climate of the Past, 12, 769–786, https://doi.org/10.5194/cp-12-769-2016, 2016.

Tetzner, D. R., Thomas, E. R., Allen, C. S., and Piermattei, A.: Evidence of Recent Active Volcanism in the Balleny Islands (Antarctica) From Ice Core Records, Journal of Geophysical Research: Atmospheres, 126, https://doi.org/10.1029/2021JD035095, _eprint: https://onlinelibrary.wiley.com/doi/pdf/10.1029/2021JD035095 tex.ids= tetzner_evidence_2021, 2021.

460 Tetzner, D. R., Thomas, E. R., Allen, C. S., and Grieman, M. M.: Regional validation of the use of diatoms in ice cores from the Antarctic Peninsula as a Southern Hemisphere westerly wind proxy, Climate of the Past, 18, 1709–1727, https://doi.org/10.5194/cp-18-1709-2022, publisher: Copernicus GmbH, 2022.

Turner, S. M., Nightingale, P. D., Broadgate, W., and Liss, P. S.: The distribution of dimethyl sulphide and dimethylsulphoniopropionate in Antarctic waters and sea ice, Deep Sea Research Part II: Topical Studies in Oceanography, 42, 1059–1080, https://doi.org/10.1016/0967-0645(95)00066-Y, 1995.

465 Udisti, R., Becagli, S., Castellano, E., Delmonte, B., Jouzel, J., Petit, J. R., Schwander, J., Stenni, B., and Wolff, E. W.: Stratigraphic correlations between the European Project for Ice Coring in Antarctica (EPICA) Dome C and Vostok ice cores showing the relative variations of snow accumulation over the past 45 kyr, Journal of Geophysical Research: Atmospheres, 109, https://doi.org/10.1029/2003JD004180, 2004.

470   Vaughan, D. G., Corr, H. F. J., Doake, C. S. M., and Waddington, E. D.: Distortion of isochronous layers in ice revealed by ground-penetrating radar, Nature, 398, 323–326, https://doi.org/10.1038/18653, number: 6725 Publisher: Nature Publishing Group, 1999.

Winstrup, M., Vallelonga, P., Kjær, H. A., Fudge, T. J., Lee, J. E., Riis, M. H., Edwards, R., Bertler, N. A. N., Blunier, T., Brook, E. J., Buizert, C., Ciobanu, G., Conway, H., Dahl-Jensen, D., Ellis, A., Emanuelsson, B. D., Hindmarsh, R. C. A., Keller, E. D., Kurbatov, A. V., Mayewski, P. A., Neff, P. D., Pyne, R. L., Simonsen, M. F., Svensson, A., Tuohy, A., Waddington, E. D., and Wheatley, S.: A 2700-year

475   annual timescale and accumulation history for an ice core from Roosevelt Island, West Antarctica, Climate of the Past, 15, 751–779, https://doi.org/https://doi.org/10.5194/cp-15-751-2019, 2019.

Wouters, B., Martin-Español, A., Helm, V., Flament, T., van Wessem, J. M., Ligtenberg, S. R. M., van den Broeke, M. R., and Bamber, J. L.: Dynamic thinning of glaciers on the Southern Antarctic Peninsula, Science, 348, 899–903, https://doi.org/10.1126/science.aaa5727, publisher: American Association for the Advancement of Science, 2015.

480   Wunderling, N., Willeit, M., Donges, J. F., and Winkelmann, R.: Global warming due to loss of large ice masses and Arctic summer sea ice, Nature Communications, 11, 5177, https://doi.org/10.1038/s41467-020-18934-3, 2020.